Chemical Engineering Science 247 (2022) 116898

Contents lists available at ScienceDirect

Chemical Engineering Science

journal homepage: www.elsevier.com/locate/ces

Superior reactivity of ferroelectric Bi_2WO_6/aluminum metastable intermolecular composite

Feiyu Xu [a,b], Benjamin Hirt [c], Prithwish Biswas [a], Dylan J. Kline [a,b], Yong Yang [a,b], Haiyang Wang [a], Alp Sehirlioglu [c], Michael R. Zachariah [a,*]

[a] Department of Chemical and Environmental Engineering, University of California, Riverside, CA 92521, United States
[b] Department of Chemistry and Biochemistry and Department of Chemical and Biomolecular Engineering, University of Maryland, College Park, MD 20742, United States
[c] Department of Materials Science and Engineering, Case Western Reserve University, Cleveland, OH 44106, United States

HIGHLIGHTS

- Piezoelectric bismuth tungsten oxide (Bi_2WO_6) was studied as an oxidizer for aluminum-based nanothermites.
- The pressurization rate of Al/Bi_2WO_6 increased almost by a factor of ten compared to Al/Bi_2O_3.
- The superior reactivity is attributed to condensed phase initiation and vigorous gas release.
- Al/Bi_2WO_6 is a potential candidate for coupled piezoelectric and nanoenergetic composites.

GRAPHICAL ABSTRACT

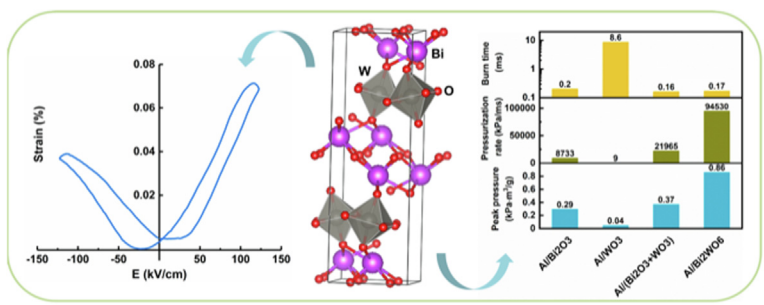

ARTICLE INFO

Article history:
Received 11 February 2021
Received in revised form 15 June 2021
Accepted 28 June 2021
Available online 1 July 2021

Keywords:
Energetic material
Metastable intermolecular composite
Piezoelectric
Combustion

ABSTRACT

Recently, the interest in exploring energetic materials beyond their basic reactive properties has grown. One such potential approach is to tune the sensitivity or reactivity by piezoelectric response to an external electric field. A wide selection of oxidizers including ferro/piezoelectric materials makes ideal candidates for such applications. Herein, ferroelectric bismuth tungstate (Bi_2WO_6) has been explored as an oxidizer for aluminum-based MICs. The reactivity of Al/Bi_2WO_6, Al/Bi_2O_3, Al/WO_3 and Al/(Bi_2O_3 + WO_3) composites was measured using a combustion cell, temperature-jump time-of-flight mass spectrometry and high-speed imaging. Al/Bi_2WO_6 shows a pressurization rate almost ten times higher than that of Al/Bi_2O_3, with a reaction that initiates in the condensed phase with a relatively low ignition temperature (920 K). The volatility of bismuth leads to vigorous release of gaseous species, which can promote heat convection and reduce reactive sintering leading to a highly reactive system.

1. Introduction

Metastable intermolecular composites (MICs), also known as nanothermites, are a class of energetic materials composed of intimately mixed nanoparticles of a fuel and an oxidizer and offer higher energy density than monomolecular energetic materials (Dreizin, 2009; Khasainov et al., 2017). The choice of nanoscale components is to decrease mass transfer resistances to enhance the energy release rate (Comet et al., 2019; Dlott, 2013; Martirosyan, 2011).

The formulation of MICs is a rather complicated topic as it involves many aspects of the fuel and oxidizer: physical properties, redox thermodynamics, particle morphology and size distribution, etc. Aluminum is the most commonly used fuel in MICs due to its high energy density and availability. A wide range of oxidizers

* Corresponding author.
E-mail address: mrz@engr.ucr.edu (M.R. Zachariah).

https://doi.org/10.1016/j.ces.2021.116898
0009-2509/

have been explored, including common metal oxides (e.g., CuO, Fe_2O_3, MoO_3, WO_3, Bi_2O_3, etc.) (Sanders et al., 2007; Wang et al., 2011; Son et al., 2007). Among this class of MICs, Al/Bi_2O_3 is particularly reactive, featuring a large pressure output and high propagation velocity (Martirosyan et al., 2009). On the other hand, Al/WO_3 produces minimal gas but has a high flame temperature. Previous research on the $Al/Fe_2O_3/WO_3$ system shows that the higher flame temperature sustained by WO_3 enhances the gasification of Fe_2O_3 and promotes the reactivity (Jacob et al., 2018). The result suggests that by integrating oxidizers that possess different attributes, enhanced reactivity can be achieved compared with the use of a single oxidizer. Thus, it is reasonable to speculate that complex metal oxides might outperform simple metal oxides in MIC formulations.

Recently, in addition to improving the performance of energetic materials by various strategies (Lyu et al., 2019; He et al., 2020a, 2020b; Wang et al., 2014; Ghildiyal et al., 2021), there are increasing interests in tuning the ignition and combustion behavior of energetic materials via external stimuli. For example, it was demonstrated that nanoaluminum/fluoropolymer reactive composites can be sensitized with the application of a DC voltage, due to the piezoelectric nature of fluoropolymers (Janesheski et al., 2012; Row and Groven, 2018). In order to explore the effect of an external electric field on MICs, the development of an electroactive energetic system is a prerequisite. Herein, a ferroelectric complex bismuth oxide – bismuth tungstate (Bi_2WO_6) – is studied as an oxidizer in the aluminum-based MIC system. The reactivity was evaluated in a combustion cell and compared with its simple metal oxide counterparts. The reaction mechanism was investigated by a fast-heating method coupled with mass spectrometry, high-speed imaging and color pyrometry, highlighting the interaction of gas generation, flame temperature and energy transfer in the course of the reaction.

2. Experimental section

2.1. Materials

Aluminum nanopowders (nAl, average size ~80 nm, 81% active by mass) were purchased from Novacentrix, bismuth nitrate ($Bi(NO_3)_3$), sodium tungstate (Na_2WO_4), bismuth oxide (Bi_2O_3, 90–210 nm), and tungsten oxide (WO_3, <100 nm) were purchase from Sigma Aldrich.

2.2. Synthesis of Bi_2WO_6

Bi_2WO_6 was synthesized by a hydrothermal method described elsewhere (Zhang and Zhu, 2005). Briefly, $Bi(NO_3)_3$ and Na_2WO_4 (1:2 M ratio) were added into DI water sequentially while stirring. White precipitate was formed, followed by sonication and washing. Then, the precipitate was placed in a Teflon lined stainless steel hydrothermal reactor (50 ml). The reactor was filled with DI water to 80% of its total volume and kept in an oven at 160 °C for 12 h. After the reaction, the product was washed with DI water and air-dried before being collected. For a typical synthesis process, 1.25 mmol Na_2WO_4 (412.31 mg) and 2.5 mmol $Bi(NO_3)_3$ (1212.68 mg) were used, and a final yield of ~50% was achieved.

2.3. Preparation of MIC samples

MICs of nAl and Bi_2O_3, WO_3, equimolar mixture of Bi_2O_3 and WO_3 (denoted as $Bi_2O_3 + WO_3$), and Bi_2WO_6 were prepared according to chemical Eqs. (1)–(4), respectively. The nAl and metal oxide powders (total amount < 50 mg) were dispersed in hexane and sonicated for 30 min to ensure sufficient mixing, followed by the evaporation of the solvent. The as-prepared Al/Bi_2WO_6 MIC was characterized by SEM (Figure S1) to ensure the homogeneous mixing of fuel and oxidizer particles. The as-prepared MIC samples are highly sensitive and reactive, thus should be handled with extreme caution!

2.4. Characterizations

Powder X-Ray Diffraction (XRD) analysis was performed on a Bruker D8 diffractometer using CuKα target (λ = 1.5418 Å). Morphology of samples were characterized by SEM (Hitachi SU-70) and TEM (JEOL JEM 2100 FEG). Energy dispersive X-ray spectroscopy was coupled with SEM to map the elemental distribution. Size distribution of samples was obtained from statistical analysis of SEM images using Nano Measurer 1.2. Simultaneous thermogravimetric (TG) and differential scanning calorimetry (DSC) was performed on a Netzsch STA 449 F3 Jupiter thermal analyzer.

2.5. Pressure cell measurements

Pressure cell tests were used to obtain the peak pressure, pressurization rate and burn time of the MICs. 25 mg of the MIC sample was put into a bowl-shaped sample holder inside a constant volume combustion cell (~20 cm^3), and was ignited by a Joule-heated nichrome coil in contact with the top of the sample (Xu et al., 2021). The combustion cell is equipped with two ports for simultaneous pressure and optical signal collection. The pressure signal is obtained by a high frequency pressure transducer (PCB Piezoelectronics). The optical emission is focused by a convex lens and transferred to a photomultiplier tube (Hamamatsu) through a fiber optic cable. Both signals are recorded by an oscilloscope.

2.6. Temperature-jump (T-Jump) time-of-flight mass spectrometry (TOFMS)

Rapid heating experiments on Al/Bi_2WO_6, $Al/(Bi_2O_3 + WO_3)$ and Bi_2WO_6 powders were performed using the T-Jump TOFMS to gain insights into the reaction mechanism. The details of the T-Jump TOFMS setup is described elsewhere (Zhou et al., 2009, Zhou et al., 2010). The samples for each of the experiments were prepared by dispersing the respective powders of Al/Bi_2WO_6, $Al/(Bi_2O_3 + WO_3)$ and Bi_2WO_6 in hexane by sonication for 30 min. The dispersion obtained after sonication (~0.1 mg sample) was uniformly coated on the center part of a platinum wire (~1 cm, d = 76 μm, OMEGA Engineering Inc.) soldered to the copper leads of the sample holder, with a micro-pipette. The prepared sample holder was then loaded into the TOFMS chamber (maintained at ~10^{-6} Torr) and the platinum wire was resistively heated with a pulsed square wave signal of ~3 ms. The current across the wire was measured by a Teledyne LeCroy CP030A 30 A 50 MHz current probe. The Callender-Van Dusen equations were used to calculate the temperature of the wire from their respective current–voltage relationship, which showed that the temperature of the wire ranges in between 1273 and 1473 K with an approximate heating rate of 10^5 K/s. The evolved reaction products upon rapid heating of the sample are ionized by a 70 eV electron gun. The positive ions produced are accelerated through the time-of-flight chamber towards the detector by an accelerator plate maintained at ~1500 V. The raw signal from the detector is collected by a Teledyne LeCroy 600 MHz oscilloscope. All of the above events consisting of rapid wire heating, ionization, and collection of spectra by the oscilloscope are synchronized with each other to obtain accurate current, voltage and time resolved spectra.

2.7. T-jump ignition characterization

The ignition behavior of the MIC samples was characterized by T-jump coupled with a high-speed camera (Vision Research Phantom V12.1). The samples were prepared the same way as described above in the T-Jump TOFMS section. Then, the sample holder was inserted into a six-way cross followed by evacuation using a vacuum pump. To probe the ignition temperature, the samples were heated by a ~3 ms pulse to ~1400 K at a heating rate of ~10^5 K/s. Meanwhile, the ignition process was recorded by the synchronized high-speed camera at 67,000 fps through an observation window. The ignition time was determined visually from optical emission of the samples and the ignition temperature was obtained correspondingly from the temperature profile of the wire.

2.8. Color camera pyrometry

The flame temperature of the MICs was measured in vacuum by a color camera pyrometry method, using the RGB filter in the camera to enable ratio pyrometry. The aforementioned rapid wire ignition of the samples was captured by a Vision Research Phantom Miro M110 color camera. To obtain an optimized result, f/11, framerate of 140,000 fps, exposure time of 6 μs were selected by trial-and-error. The video was then processed by a custom MATLAB script to give spatiotemporal temperature map of the reaction. Temperature estimation by color ratio pyrometry is based on calibration of the spectral response of the camera and other camera-specific calibration factors to estimate the ratios in different color channels (assuming graybody emission). This method is largely based on the work described by Densmore et al (Densmore et al., 2011).Using Planck's Law, one can estimate the intensity of light at a given wavelength and temperature for a radiating blackbody. By integrating over the entire light spectrum to which the camera's CMOS sensor is sensitive and incorporating the Red, Green, and Blue filter transmission from the camera's Bayer filter, we can get an expected value for Red, Green, and Blue pixels for a given temperature. To simplify this calculation and minimize error, ratios in different channels are taken to remove dependency on image capture parameters and only a calibration factor is used to correct for non-ideal responses in the sensor and camera lens. The estimated values of the different ratios and their corresponding temperature are placed in a lookup table. The video processing algorithm simply computes these ratios at each pixel location in the image and estimates the temperature based on the measured color ratios and those in the lookup table. More details regarding this method can be found in our previous work (Jacob et al., 2018).

3. Results and discussion

3.1. Characterizations of Bi_2WO_6

Bi_2WO_6 is the simplest member of the Aurivillius phase family, comprising alternating $Bi_2O_2^{2+}$ layers and pseudo-perovskite WO_4^{2-} layers (Figure S2) (Zhang et al., 2011). Aurivillius phases have been studied as lead-free piezoelectric materials and oxide ion conductors (Moure, 2018; Kendall et al., 1996; Saiful Islam et al., 1998). Bi_2WO_6 used in this study was synthesized via a hydrothermal method (Zhang and Zhu, 2005). As shown in Fig. 1a, XRD of the as-synthesized Bi_2WO_6 can be indexed to an orthorhombic Bi_2WO_6 phase without any impurity phase. Because of the particular layered crystal structure, the lateral crystal growth of Bi_2WO_6 is favored, and results in an anisotropic morphology. SEM (Fig. 1b) and TEM (Fig. 1c) characterizations show square-like Bi2WO6 platelets. The SEM image was further analyzed statistically using Nano Measurer to obtain the size distribution of nanoparticles, as shown in Fig. 1d. The edge length of the platelets ranges from 40 to 240 nm, with an average of 90 nm.

As one of the motivating factors in using Bi_2WO_6 was to introduce piezoelectric powders into the combusting system, we verified the piezoelectricity of the material on pellets processed by conventional sintering using the parameters described elsewhere (Zeng et al., 2015). The bulk samples were polished and electroded with air-dry silver paint. Poling was performed in a silicone oil bath and poled with DC current at 120 kV/cm at 80 °C with a 5-minute voltage ramp up and 15-minute hold. Piezoelectric properties (d_{33}) were characterized by TF2000 ferroelectric analyzer (aixACCT, Aachen, Germany) coupled with a laser-doppler vibrometer (Polytec OFV-5000, Waldbronn, Germany). While piezoelectric coefficients (d_{33}) were measured for polycrystalline (9.2–14 pC/N after conventional sintering (Zeng et al., 2015; Liao et al., 2016); 15 pC/N after spark plasma sintering (Zeng et al., 2009) and single crystalline (27 pC/N) (Takeda et al., 2010) Bi_2WO_6, it was either through the use of a quasi-static d_{33}-meter (polycrystalline) or resonance measurements (single crystalline). The converse high field piezoelectric properties have never been reported to our knowledge. One reason for this is the high leakage current and relatively low breakdown of these materials at electric fields close to the poling and measurement fields (Yanovskii and Voronkova, 1986). While we are reporting the piezoelectric behavior here, it should be noted that many samples experienced electric breakdown around 130 kV/cm during the measurements.

Fig. 2 shows the high field induced strain for Bi_2WO_6 polycrystalline samples at room temperature. The asymmetry indicated that there is domain pinning in the system that forms during poling possibly due to diffusion of oxygen vacancies, which are known to exist in these materials leading to fast oxygen ion transport, to the domain walls (Utkin et al., 1980). The d_{33}^* calculated as maximum strain to maximum electric field ratio was 56 pm/V.

3.2. Reactivity of Al/Bi_2WO_6 composite

The reactivity of the MICs was tested in a constant volume combustion cell (Sullivan and Zachariah, 2010). In a typical measurement, the composite is ignited in the combustion cell and the pressure and optical signals are recorded simultaneously. The pressure signal indicates gas release and temperature increase, and the optical emission is a reasonable measure of the duration of the reaction. Stoichiometric Al/Bi_2WO_6 composite was prepared according to chemical equation (1):

$$4Al + Bi_2WO_6 \rightarrow 2Al_2O_3 + 2Bi + W \quad (1)$$

A fixed amount of loosely-packed powder of Al/Bi_2WO_6 sample was used in each test. Fig. 3a shows a typical pressure rise profile and optical emission profile of Al/Bi_2WO_6 samples versus time. The slope of the pressure rise is defined as pressurization rate and the full width at half maximum (FWHM) of optical emission intensity is taken as burn time. In Fig. 3a, the pressure increases dramatically to over 1000 kPa within about 0.01 ms, indicating vigorous and rapid gas generation after initiation of the reaction. The burn time is determined to be 0.17 ms.

The particle size of the oxidizer plays an important role in the propagation of nanothermite reaction. Weismiller et al. (Weismiller et al., 2011) showed that reducing the size decreases the timescale of heating associated with the decomposition and vaporization of oxide particles, and the length scale is also shorter for gas to diffuse away from particles, both leading to a higher local pressurization rate and an enhancement of overall convective propagation. This implies that the reaction may benefit from the nanoscale size of Bi_2WO_6 particles.

For comparison purposes, other oxidizers were also selected and tested with nano-Al in the combustion cell, including Bi_2O_3,

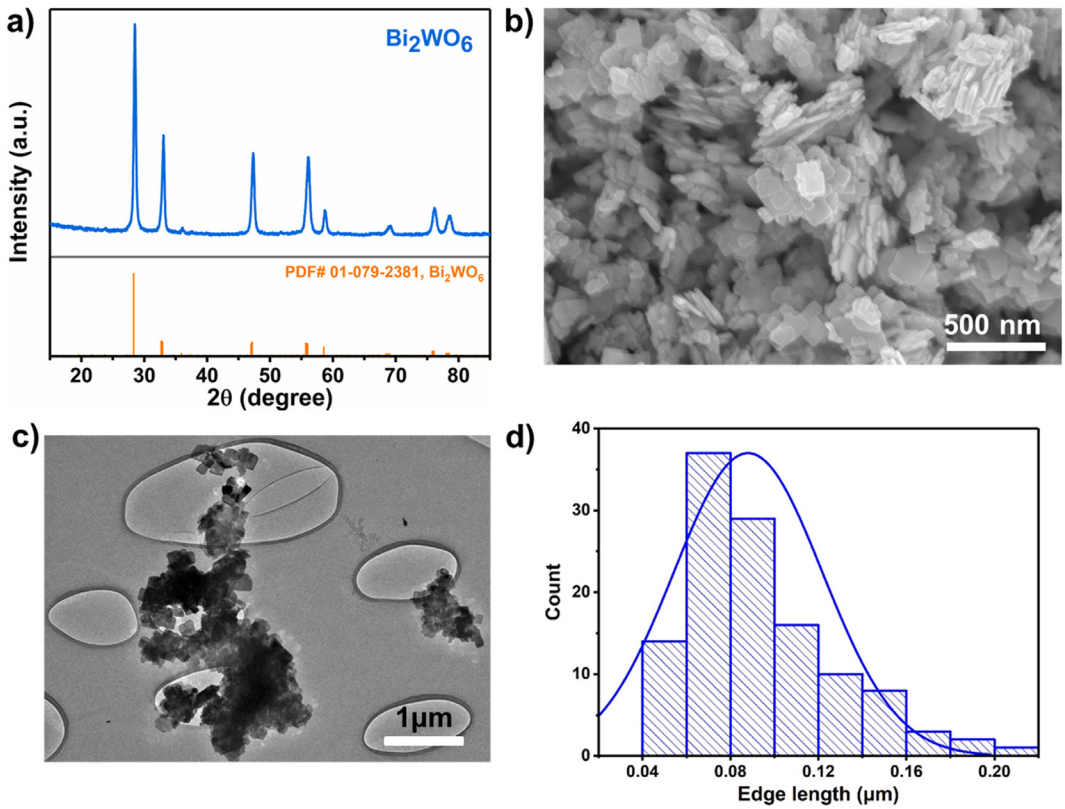

Fig. 1. (a) XRD of as-prepared Bi_2WO_6 which is indexed to an orthorhombic phase. (b) SEM and (c)TEM images show Bi_2WO_6 nanoplatelets. (d) Size distribution of Bi_2WO_6 with an average edge length of 90 nm.

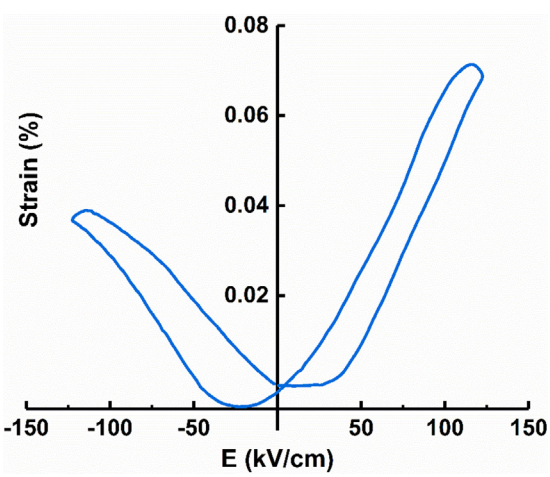

Fig. 2. High electric field induced strain in polycrystalline Bi_2WO_6. The engineering d_{33}^* calculated as maximum strain to maximum electric field ratio was 56 pm/V.

WO_3 and equimolar physical mixture of Bi_2O_3 + WO_3. The first two are simple oxide components of Bi_2WO_6, while the last one has the same chemical composition as Bi_2WO_6. The corresponding MICs were prepared according to Eqs. (2)–(4), respectively.

$$2Al + Bi_2O_3 \rightarrow Al_2O_3 + 2Bi \quad (2)$$

$$2Al + WO_3 \rightarrow Al_2O_3 + W \quad (3)$$

$$4Al + Bi_2O_3 + WO_3 \rightarrow 2Al_2O_3 + 2Bi + W \quad (4)$$

The pressure profiles of Al/Bi_2O_3, Al/Bi_2O_3 + WO_3, Al/Bi_2WO_6 are plotted in Fig. 3b, with the inset showing the zoomed-in plot of the initial rise and total pressure rise time. Since Al/WO_3 is known to generate minimal gas, it is not shown. The pressure rise time of Al/Bi_2O_3 is 0.12 ms, while the pressurization time of Al/Bi_2O_3 + WO_3 is only half of that. The peak pressure of Al/Bi_2O_3 + WO_3 is also slightly higher than that of Al/Bi_2O_3, suggesting that more gas is generated within a shorter time after the addition of WO_3. This result is in accordance with previous study of Al/Fe_2O_3/WO_3 system that shows the higher flame temperature sustained by WO_3 enhances the gasification of Fe_2O_3 (Jacob et al., 2018). Noticeably, the peak pressure of Al/Bi_2WO_6 is almost three times as high as that of Al/Bi_2O_3, and the pressurization rate is more than ten times higher. This demonstrates that Al/Bi_2WO_6 is a superior gas generator and the gasification of reactants and products is highly efficient.

A complete comparison of peak pressure, pressurization peak and burn time of the abovementioned samples is shown in Fig. 3c. Al/WO_3 shows significantly lower peak pressure and pressurization rate as well as longer burn time, compared to the other three systems. This is expected due to lack of gaseous products (Jacob et al., 2018). In contrast, Al/Bi_2O_3 is one of the most reactive MICs known and can be used a reference (Wang et al., 2011). As shown in Fig. 3c, Al/Bi_2WO_6 exhibits considerably better reactivity than Al/Bi_2O_3: the peak pressure is 3 times as high as Al/Bi_2O_3, the pressurization rate is 10 times higher and the burn time is about 20% shorter. The fact that Al/Bi_2WO_6 outperforms Al/Bi_2O_3 indicates that Bi_2WO_6 is a superior oxidizer for Al-based nanothermite system.

Stoichiometry can also significantly affect the reactivity of MICs (Dutro et al., 2009). The peak pressure, pressurization rate and burn time of Al/Bi_2WO_6 composite with different stoichiometry are shown in Fig. 3d. The stoichiometric mixture shows the highest peak pressure, pressurization rate and the shortest burn time. Shifting the stoichiometry to either fuel lean or rich decreases the overall reactivity as expected.

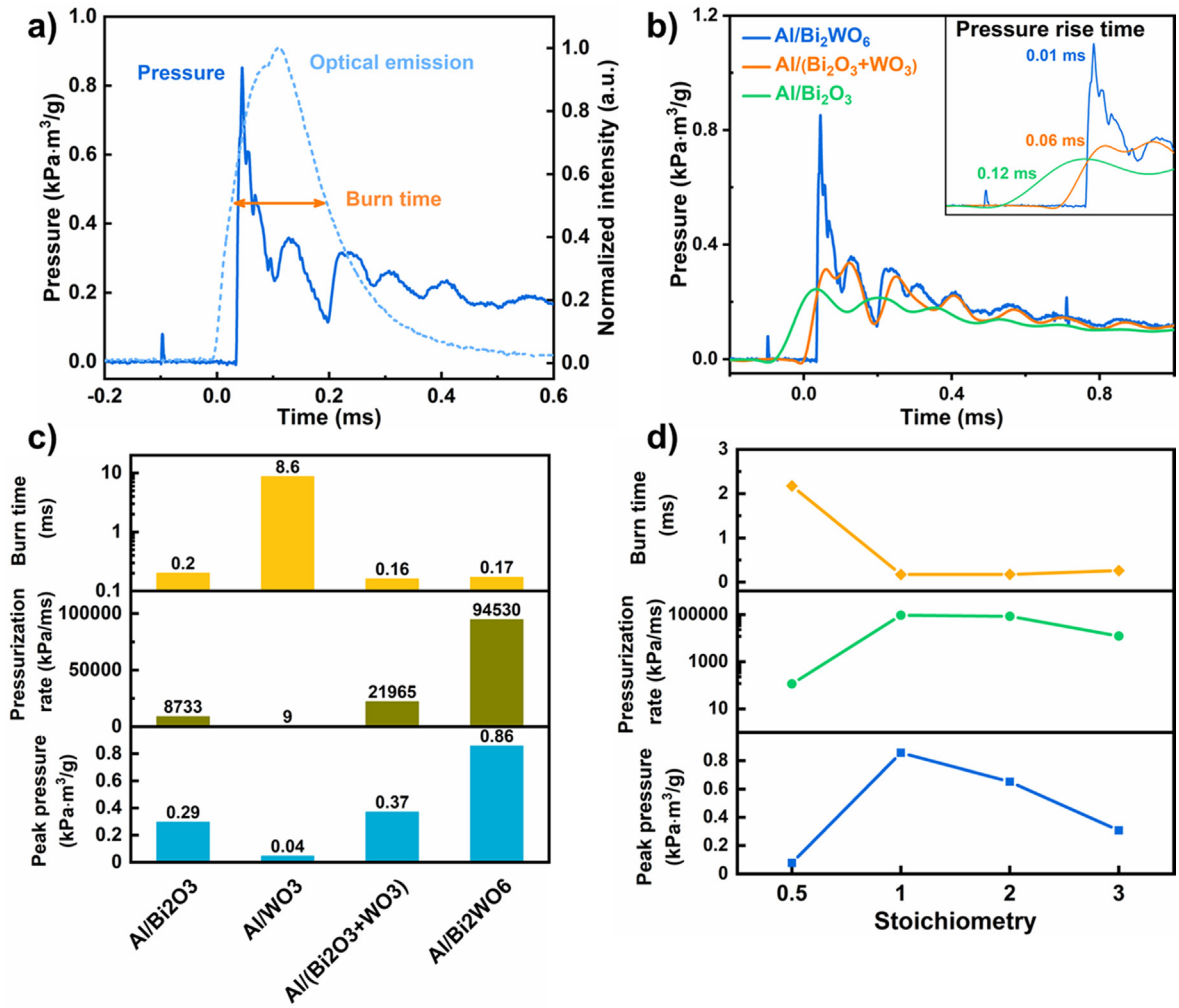

Fig. 3. (a) Typical pressure and optical emission profile of Al/Bi_2WO_6 composites. (b) Comparison of pressure rise of Al/Bi_2WO_6, $Al/(Bi_2O_3 + WO_3)$ and Al/Bi_2O_3. Inset: Zoomed-in plot of the initial part and pressure rise time. (c) Peak pressure, pressurization rate and burn time of Al/Bi_2WO_6, $Al/(Bi_2O_3 + WO_3)$, Al/Bi_2O_3 and $Al/(WO_3)$. (d) Peak pressure, pressurization rate and burn time of Al/Bi_2WO_6 with varying stoichiometry.

3.3. Reaction mechanism

3.3.1. Rapid heating measurements

Temperature-Jump Time-of-Flight Mass Spectrometry (T-Jump TOFMS) was used to probe the initiation of the reaction between Al and Bi_2WO_6. The temporal nature of this method enables the measurement of time and temperature of different species produced throughout the duration of the reaction. The time-resolved release of reaction intermediates and products reveals important information about the initiation of a reaction (Zhou et al., 2009; Zhou et al., 2010).

The summary plot of the mass spectrum of Al/Bi_2WO_6 reaction is shown in Figure S3. Peaks of species from background (H_2O^+, N_2^+), reaction intermediates (Al^+, AlO^+) and products (Bi^+, Bi^{2+}) can be observed. In order to gain more insights into the reaction kinetics of Al/Bi_2WO_6, the time-resolved evolution of a reaction product, bismuth (Bi), was studied. Bi (m/z = 209) was selected because of its volatile nature. The normalized intensity of Bi signal versus time was plotted for Al/Bi_2WO_6, $Al/(Bi_2O_3 + WO_3)$ and neat Bi_2WO_6 samples as shown in Fig. 4a. The two thermite mixtures start to release Bi at approximately the same time, but Al/Bi_2WO_6 reaches its peak intensity much earlier than $Al/(Bi_2O_3 + WO_3)$. This indicates that Al/Bi_2WO_6 generates Bi faster, consistent with the higher pressurization rate discussed earlier. The appearance of Bi due to the thermal decomposition of Bi_2WO_6 occurs much later at about the same time as oxygen release.

Previous studies on mechanisms of nanothermite reactions show that some reactions, such as Al/CuO and Al/Fe_2O_3, initiate at a time and temperature close to that of oxygen release from neat oxidizer. On the other hand, for some reactions such as Al/Bi_2O_3, initiation of the reaction precedes the release of gaseous oxygen, suggesting that the reaction initiates in the condensed phase (Jian et al., 2013; Piekiel et al., 2014). These conclusions were made by comparison of the thermal decomposition behavior of the oxidizer and ignition temperature of the thermite reaction. In order to study the role that oxidizer plays in the initiation of Al/Bi_2WO_6 reaction, the decomposition behavior of Bi_2WO_6 was characterized. Fig. 4b shows the temporal variation of the oxygen (m/z = 32) signal intensity and the temperature of the wire. The oxygen release from Bi_2WO_6 due to thermal decomposition occurs around 2.7 ms at a temperature of ~1298 K. The decomposition of Bi_2WO_6 is further confirmed by TGA at low heating rate (Figure S4), which shows an onset temperature of ~1300 K. Both results suggest that Bi_2WO_6 is thermally stable and does not release oxygen below ~1300 K.

The ignition behavior of Al/Bi_2WO_6 composite was studied by T-jump coupled with a high-speed camera. The experiment was conducted in vacuum with a very small amount of sample (~0.1 mg)

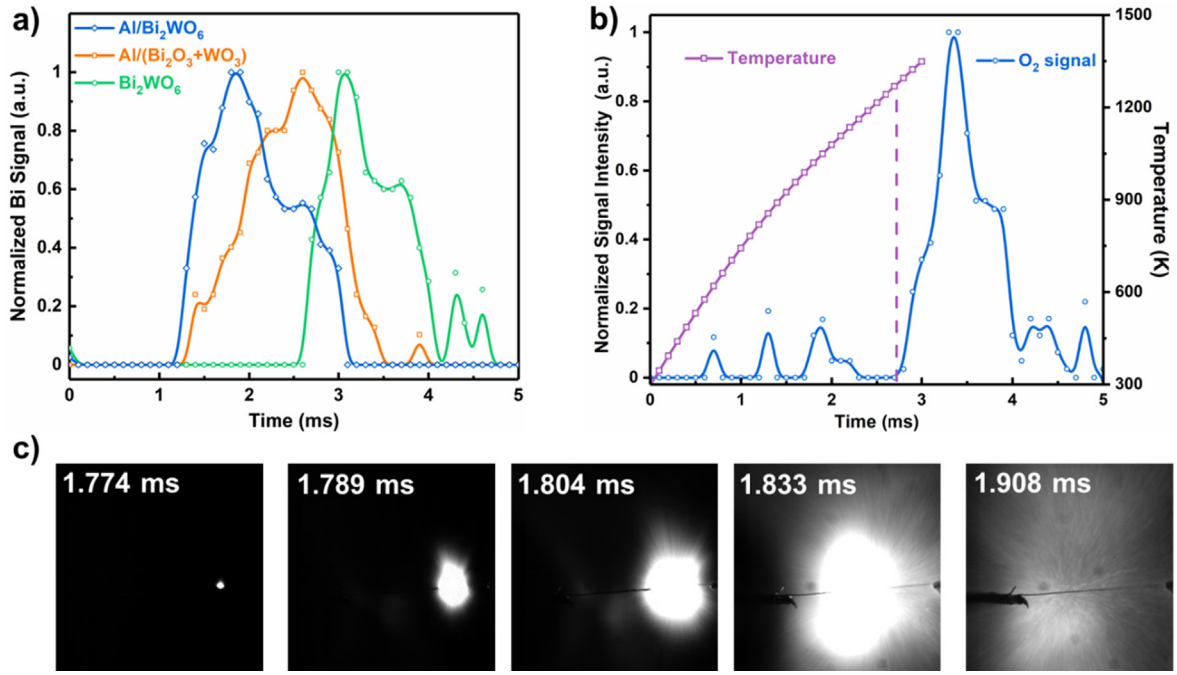

Fig. 4. T-jump TOFMS and ignition experiments. (a) Bi signal (m/z = 209) of Al/Bi_2WO_6, Al/(Bi_2O_3 + WO_3) and Bi_2WO_6 versus time. (b) Oxygen (m/z = 32) signal and wire temperature versus time. (c) Snapshots of Al/Bi_2WO_6 wire ignition video recorded by a high-speed camera.

coated on the platinum wire. The temperature profile and high-speed video are recorded simultaneously upon triggering the heating of the wire. The time of ignition can be determined from the video and the corresponding temperature can be obtained from the temperature profile. In this case, the ignition temperature of Al/Bi_2WO_6 was determined to be 923 ± 10 K, which is significantly lower than the oxygen release temperature of Bi_2WO_6 (~1298 K). Furthermore, the Bi signal of Al/Bi_2WO_6 reaction (~1.2 ms) also appears much earlier than Bi_2WO_6 decomposition (~2.7 ms). Therefore, it is evident that the reaction initiates prior to the release of molecular oxygen and is thus in the condensed phase. Some studies have shown that for nanothermite composites, oxygen ion conductivity is vital to the condensed phase initiation of reaction (Wang et al., 2017; Wang et al., 2016). The unique oxygen ion transport behavior was also suggested to assist in the violent reaction of Al/Bi_2O_3 nanothermite (Piekiel et al., 2014). In this regard, Bi_2WO_6 has been recognized as a good oxide ion conductor (Kendall et al., 1996; Takahashi and Iwahara, 1973), which might contribute to the rapid initiation of the reaction.

The snapshots of Al/Bi_2WO_6 reaction captured by high-speed camera are shown in Fig. 4c. Upon ignition, the size of the reaction area starts to increase dramatically in a short duration of time. The reaction propagates radially as well as along the wire before it dies. For aluminum-based thermites, aggregates of particles caused by reactive sintering is a common issue and negatively affects the reactivity (Sullivan et al., 2012). However, the reaction of Al/Bi_2WO_6 propagates homogenously and no spark was observed, indicating that the extent of sintering is not significant.

3.3.2. Reaction temperature

Flame temperature was obtained by a high-speed color camera pyrometry (Jacob et al., 2018). The snapshots of the color camera video and spatiotemporal temperature map of Al/Bi_2WO_6 and Al/(Bi_2O_3 + WO_3) are shown in Fig. 5a and 5b, respectively. Within 0.04 ms, Al/Bi_2WO_6 produced a large cloud of reacted material compared with Al/(Bi_2O_3 + WO_3), indicating vigorous reaction and the presence of a large amount of gaseous species. In the temperature map, a transition of colors (i.e., from yellow to green to blue) from the center to the periphery of the reaction area suggests a decreasing temperature gradient. This could be a sign of enhanced convective heat transfer, as Al/(Bi_2O_3 + WO_3) shows no distinguishable temperature gradient. This result is in agreement with the higher reactivity of Al/Bi_2WO_6 shown by the pressure cell results.

The measured flame temperature for Al/Bi_2WO_6 is ~2960 K as shown in Figure S5, and the corresponding calculated adiabatic flame temperature by CHEETAH code is shown in Table 1. Previous work by Jacob et al. showed that a higher flame temperature enhances the gasification of unreacted materials and increases the reactivity of nanothermite composites (Jacob et al., 2018). In this case, Al/Bi_2WO_6 has a higher flame temperature compared to Al/Bi_2O_3, presumably because Al/WO_3 also has a high flame temperature (~3360 K). Higher temperatures will also nominally result in a higher pressurization rate. It is often found that, although nanothermites are intimately mixed and highly reactive, some nanothermite reactions may not reach completion due to severe sintering of reactants (Jacob et al., 2017), and the flame temperature is an important indicator of the extent of completion. The high measured temperature relative to the adiabatic temperature implies that the reaction is approaching the thermodynamic limit of completion. This is likely because the condensed phase dominated reaction is more efficient compared with gas phase reactions, especially for such a short timescale (Jacob et al., 2017), and the high oxygen ion conductivity would seem to promote rapid reaction (Piekiel et al., 2014; Wang et al., 2017).

In nanothermite reactions, propagation is largely determined by the ignition threshold and heat transfer properties. A low ignition temperature and efficient heat transfer will greatly benefit propagation (Wang et al., 2019). As demonstrated by the T-jump experiments, the reaction between Al and Bi_2WO_6 initiates in the condensed phase, further facilitated by the high oxygen ion conductivity of Bi_2WO_6, leading to a low ignition temperature. During the reaction, bismuth is produced and vaporized rapidly due to its low boiling point (1837 K) relative to the flame temperature

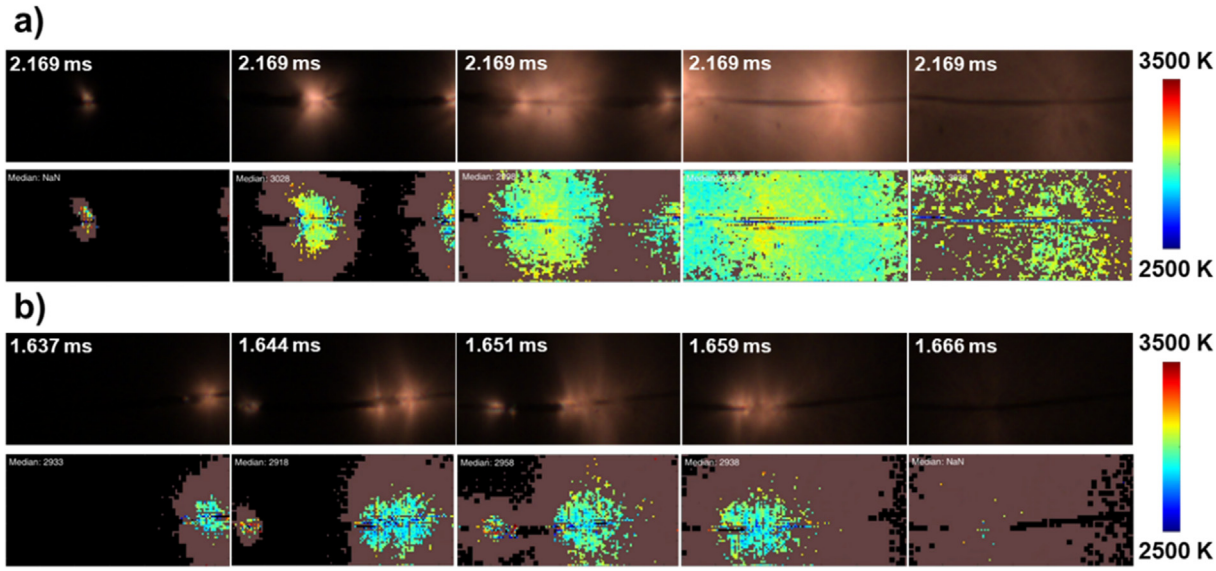

Fig. 5. Color camera images and temperature map of Al/Bi_2WO_6 (a) and Al/(Bi_2O_3 + WO_3) (b). The top image of each figure is the original image and the bottom one is the temperature map. The corresponding time is shown at the bottom of each image.

Table 1
Adiabatic flame temperature calculated by CHEETAH.

Al-based nanothermites	Adiabatic flame temperature (K)
Bi_2O_3	2459
WO_3	3362
Bi_2O_3 + WO_3	2919
Bi_2WO_6	2903

(~2960 K). The convection and condensation of substantial gaseous bismuth can play an important role in heat transfer (Egan and Zachariah, 2015). In addition, the gas generation disaggregate the unreacted material, thus reducing the reactive sintering effect. As a result, the ignition and heat transfer of the reaction are both enhanced and create a positive feedback leading to high reactivity.

3.3.3. Combustion products analysis

In order to verify the proposed reaction mechanism, the combustion products of Al/Bi_2WO_6 composite were collected from the combustion cell. SEM images (Fig. 6a and S6) of the products show two populations of particles with distinct size distribution. The majority of the particles have a size smaller than 100 nm, with only a few micro-sized particles. To investigate the nature of two different particles populations, elemental mapping of the combustion products was obtained by EDS. As shown in Fig. 6a and b, the large micro-sized particles are rich in Al and O and thus should be aluminum oxide, indicative of reactive sintering. It also shows

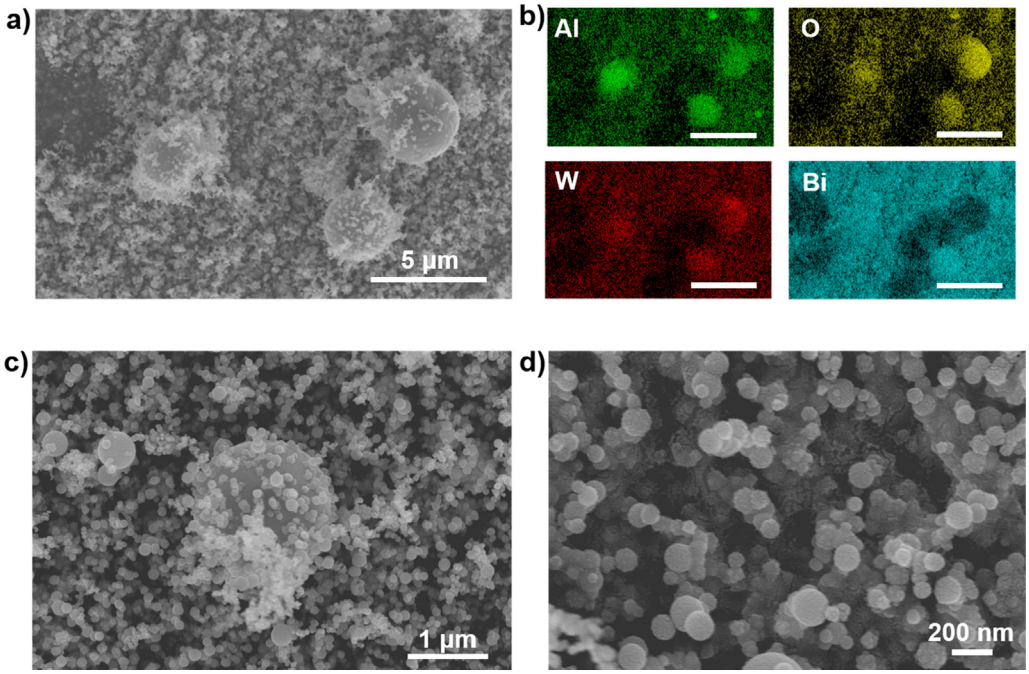

Fig. 6. SEM image (a) and EDS element mapping (b) of the combustion product of Al/Bi_2WO_6. The scale bar in (b) is 5 μm. (c) and (d) Zoomed-in images of the combustion product.

slightly higher W signal, possibly because W cannot be vaporized (b.p. = 5555 K) and stays in the condensed phase, becoming part of the large particle upon quenching. The small particles are mainly composed of Bi as evidenced by the elemental mapping. From the zoomed-in image (Fig. 6c and d), it can be observed that the surface of the large particle is partially covered by some small particles. No platelet-shaped particles can be observed in the combustion product, implying that Bi_2WO_6 was fully reacted, or at least underwent phase change that destroyed the original morphology. Further examination shows that the particles are all highly regular spheres, suggesting that they are likely formed by solidification of molten state or vapor condensation (Jacob et al., 2015). The fine spherical shape and uniform particle size distribution validates the vigorous gasification during the reaction.

4. Conclusions

The formulation of a powerful MIC, Al/Bi_2WO_6, was developed by incorporating a ferroelectric material as an oxidizer. Al/Bi_2WO_6 is highly reactive as evidenced by a pressurization rate almost ten times higher than that of Al/Bi_2O_3. T-jump mass spectrometry and high-speed imaging results show that the reaction initiates in the condensed phase followed by rapid generation of gaseous products, which is enhanced by the high flame temperature. The vigorous gas release can improve heat transfer and mitigate the reactive sintering effect, thus increasing the overall reactivity. Al/Bi_2WO_6 can serve as a promising candidate for coupled piezoelectric and nanoenergetic composites.

Declaration of Competing Interest

The authors declare that they have no known competing financial interests or personal relationships that could have appeared to influence the work reported in this paper.

Acknowledgements

This work was supported by Office of AFOSR MURI Program.

Appendix A. Supplementary material

Supplementary data to this article can be found online at https://doi.org/10.1016/j.ces.2021.116898.

References

Comet, M., Martin, C., Schnell, F., Spitzer, D., 2019. Nanothermites: a short review. factsheet for experimenters, present and future challenges, Propellants Explos. Pyrotech. 44, 18–36. https://doi.org/10.1002/prep.201800095.

Densmore, J.M., Biss, M.M., McNesby, K.L., Homan, B.E., 2011. High-speed digital color imaging pyrometry. Appl. Opt. 50, 2659–2665. https://doi.org/10.1364/AO.50.002659.

Dlott, D.D., 2013. Thinking big (and small) about energetic materials. Mater. Sci. Technol. 22, 463–473. https://doi.org/10.1179/174328406x83987.

Dreizin, E.L., 2009. Metal-based reactive nanomaterials. Prog. Energy Combust. Sci. 35, 141–167. https://doi.org/10.1016/j.pecs.2008.09.001.

Dutro, G.M., Yetter, R.A., Risha, G.A., Son, S.F., 2009. The effect of stoichiometry on the combustion behavior of a nanoscale Al/MoO3 thermite. Proc. Combust. Inst. 32, 1921–1928. https://doi.org/10.1016/j.proci.2008.07.028.

Egan, G.C., Zachariah, M.R., 2015. Commentary on the heat transfer mechanisms controlling propagation in nanothermites. Combust. Flame 162, 2959–2961. https://doi.org/10.1016/j.combustflame.2015.04.013.

Ghildiyal, P., Ke, X., Biswas, P., Nava, G., Schwan, J., Xu, F., Kline, D.J., Wang, H., Mangolini, L., Zachariah, M.R., 2021. Silicon nanoparticles for the reactivity and energetic density enhancement of energetic-biocidal mesoparticle composites. ACS Appl. Mater. Interfaces. 13, 458–467. https://doi.org/10.1021/acsami.0c17159.

He, W., Ao, W., Yang, G., Yang, Z., Guo, Z., Liu, P.-J., Yan, Q.-L., 2020a. Metastable energetic nanocomposites of MOF-activated aluminum featured with multi-level energy releases. Chem. Eng. J. 381,. https://doi.org/10.1016/j.cej.2019.122623 122623.

He, W., Li, Z.-H., Chen, S., Yang, G., Yang, Z., Liu, P.-J., Yan, Q.-L., 2020b. Energetic metastable n-Al@PVDF/EMOF composite nanofibers with improved combustion performances. Chem. Eng. J. 383,. https://doi.org/10.1016/j.cej.2019.123146 123146.

Jacob, R.J., Jian, G., Guerieri, P.M., Zachariah, M.R., 2015. Energy release pathways in nanothermites follow through the condensed state. Combust. Flame 162, 258–264. https://doi.org/10.1016/j.combustflame.2014.07.002.

Jacob, R.J., Ortiz-Montalvo, D.L., Overdeep, K.R., Weihs, T.P., Zachariah, M.R., 2017. Incomplete reactions in nanothermite composites. J. Appl. Phys. 121. https://doi.org/10.1063/1.4974963.

Jacob, R.J., Kline, D.J., Zachariah, M.R., 2018. High speed 2-dimensional temperature measurements of nanothermite composites: probing thermal vs. gas generation effects. J. Appl. Phys. 123. https://doi.org/10.1063/1.5021890.

Janesheski, R.S., Groven, L.J., Son, S., 2012. Fluoropolymer and aluminum piezoelectric reactives. AIP Conf. Proc. 1426, 741–744. https://doi.org/10.1063/1.3686385.

Jian, G., Chowdhury, S., Sullivan, K., Zachariah, M.R., 2013. Nanothermite reactions: Is gas phase oxygen generation from the oxygen carrier an essential prerequisite to ignition? Combust. Flame 160, 432–437. https://doi.org/10.1016/j.combustflame.2012.09.009.

Kendall, K.R., Navas, C., Thomas, J.K., zur Loye, H.-C., 1996. Recent developments in oxide ion conductors: aurivillius phases, Chem. Mater. 8, 642–649. https://doi.org/10.1021/cm9503083.

Khasainov, B., Comet, M., Veyssiere, B., Spitzer, D., 2017. Comparison of performance of fast-reacting nanothermites and primary explosives. Propellants Explos. Pyrotech. 42, 754–772. https://doi.org/10.1002/prep.201600181.

Liao, Q., An, Z., Huang, H., Fang, M., Chen, Z., Peng, S., Li, K., 2016. Ultra-high Curie temperature (>800 °C) low sintering temperature Bi2(1–x)La2xWO6 piezoelectric material for the applications of seafloor hydrothermal vents detection. Smart Mater. Struct. 25. https://doi.org/10.1088/0964-1726/25/10/10lt03.

Lyu, J.-Y., Chen, S., He, W., Zhang, X.-X., Tang, D., Liu, P.-J., Yan, Q.-L., 2019. Fabrication of high-performance graphene oxide doped PVDF/CuO/Al nanocomposites via electrospinning. Chem. Eng. J. 368, 129–137. https://doi.org/10.1016/j.cej.2019.02.170.

Martirosyan, K.S., 2011. Nanoenergetic gas-generators: principles and applications. J. Mater. Chem. 21. https://doi.org/10.1039/c1jm11300c.

Martirosyan, K.S., Wang, L., Vicent, A., Luss, D., 2009. Synthesis and performance of bismuth trioxide nanoparticles for high energy gas generator use. Nanotechnology 20,. https://doi.org/10.1088/0957-4484/20/40/405609 405609.

Moure, A., 2018. Review and perspectives of aurivillius structures as a lead-free piezoelectric system. Appl. Sci. 8. https://doi.org/10.3390/app8010062.

Piekiel, N.W., Zhou, L., Sullivan, K.T., Chowdhury, S., Egan, G.C., Zachariah, M.R., 2014. Initiation and reaction in Al/Bi2O3 nanothermites: evidence for the predominance of condensed phase chemistry. Combust. Sci. Technol. 186, 1209–1224. https://doi.org/10.1080/00102202.2014.908858.

Row, S.L., Groven, L.J., 2018. Smart energetics: sensitization of the aluminum-fluoropolymer reactive system. Adv. Eng. Mater. 20. https://doi.org/10.1002/adem.201700409.

Saiful Islam, M., Lazure, S., Vannier, R., Nowogrocki, G., Mairesse, G., 1998. Structural and computational studies of Bi2WO6 based oxygen ion conductors. J. Mater. Chem. 8, 655–660. https://doi.org/10.1039/A707221J.

Sanders, V.E., Asay, B.W., Foley, T.J., Tappan, B.C., Pacheco, A.N., Son, S.F., 2007. Reaction propagation of four nanoscale energetic composites (Al/MoO3, Al/WO3, Al/CuO, and B12O3). J. Propuls. Power. 23, 707–714. https://doi.org/10.2514/1.26089.

Son, S.F., Asay, B.W., Foley, T.J., Yetter, R.A., Wu, M.H., Risha, G.A., 2007. Combustion of nanoscale Al/MoO3 thermite in microchannels. J. Propuls. Power. 23, 715–721. https://doi.org/10.2514/1.26090.

Sullivan, K.T., Piekiel, N.W., Wu, C., Chowdhury, S., Kelly, S.T., Hufnagel, T.C., Fezzaa, K., Zachariah, M.R., 2012. Reactive sintering: an important component in the combustion of nanocomposite thermites. Combust. Flame 159, 2–15. https://doi.org/10.1016/j.combustflame.2011.07.015.

Sullivan, K., Zachariah, M., 2010. Simultaneous pressure and optical measurements of nanoaluminum thermites: investigating the reaction mechanism. J. Propuls. Power. 26, 467–472. https://doi.org/10.2514/1.45834.

Takahashi, T., Iwahara, H., 1973. High oxide ion conduction in sintered oxides of the system Bi2O3-WO3. J. Appl. Electrochem. 3, 65–72. https://doi.org/10.1007/bf01119469.

Takeda, H., Han, J.S., Nishida, M., Shiosaki, T., Hoshina, T., Tsurumi, T., 2010. Growth and piezoelectric properties of ferroelectric Bi2WO6 mono-domain crystals. Solid State Commun. 150, 836–839. https://doi.org/10.1016/j.ssc.2010.02.011.

Utkin, V.I., Roginskaya, Yu.E., Voronkova, V.I., Yanovskii, V.K., Galyamov, B.Sh., Venevtsev, Yu.N., 1980. Dielectric properties, electrical conductivity, and relaxation phenomena in ferroelectric Bi2WO6. Phys. Status Solidi A 59, 75–82. https://doi.org/10.1002/pssa.2210590110.

Wang, H., Jian, G., Egan, G.C., Zachariah, M.R., 2014. Assembly and reactive properties of Al/CuO based nanothermite microparticles. Combust. Flame 161, 2203–2208. https://doi.org/10.1016/j.combustflame.2014.02.003.

Wang, H., Kline, D.J., Rehwoldt, M., Wu, T., Zhao, W., Wang, X., Zachariah, M.R., 2019. Architecture can significantly alter the energy release rate from nanocomposite energetics. ACS Appl. Polym. Mater. 1, 982–989. https://doi.org/10.1021/acsapm.9b00016.

Wang, L., Luss, D., Martirosyan, K.S., 2011. The behavior of nanothermite reaction based on Bi2O3/Al. J. Appl. Phys. 110. https://doi.org/10.1063/1.3650262.
Wang, X., Wu, T., Zachariah, M.R., 2016. Doped perovskites to evaluate the relationship between fuel-oxidizer thermite ignition and bond energy, electronegativity, and oxygen vacancy. J. Phys. Chem. C 121, 147–152. https://doi.org/10.1021/acs.jpcc.6b10571.
Wang, X., Zhou, W., DeLisio, J.B., Egan, G.C., Zachariah, M.R., 2017. Doped delta-bismuth oxides to investigate oxygen ion transport as a metric for condensed phase thermite ignition. Phys. Chem. Chem. Phys. 19, 12749–12758. https://doi.org/10.1039/c6cp08532f.
Weismiller, M.R., Malchi, J.Y., Lee, J.G., Yetter, R.A., Foley, T.J., 2011. Effects of fuel and oxidizer particle dimensions on the propagation of aluminum containing thermites. Proc. Combust. Inst. 33, 1989–1996. https://doi.org/10.1016/j.proci.2010.06.104.
Xu, F., Biswas, P., Nava, G., Schwan, J., Kline, D.J., Rehwoldt, M.C., Mangolini, L., Zachariah, M.R., 2021. Tuning the reactivity and energy release rate of I2O5 based ternary thermite systems. Combust. Flame 228, 210–217. https://doi.org/10.1016/j.combustflame.2020.12.047.
Yanovskii, V.K., Voronkova, V.I., 1986. Polymorphism and properties of Bi2WO6 and Bi2MoO6. Phys. Status Solidi A 93, 57–66. https://doi.org/10.1002/pssa.2210930106.
Zeng, T., Yan, H., Ning, H., Zeng, J., Reece, M.J., 2009. Piezoelectric and ferroelectric properties of bismuth tungstate ceramics fabricated by spark plasma sintering. J. Am. Ceram. Soc. 92, 3108–3110. https://doi.org/10.1111/j.1551-2916.2009.03344.x.
Zeng, T., Yu, X., Hui, S., Zhou, Z., Dong, X., 2015. Structural and electrical properties of Bi2WO6 piezoceramics prepared by solid state reaction method. Mater. Res. Bull. 68, 271–275. https://doi.org/10.1016/j.materresbull.2015.04.004.
Zhang, L., Wang, H., Chen, Z., Wong, P.K., Liu, J., 2011. Bi2WO6 micro/nano-structures: synthesis, modifications and visible-light-driven photocatalytic applications. Appl. Catal. B Environ. https://doi.org/10.1016/j.apcatb.2011.05.008.
Zhang, C., Zhu, Y., 2005. Synthesis of square Bi2WO6 nanoplates as high-activity visible-light-driven photocatalysts. Chem. Mater. 17, 3537–3545. https://doi.org/10.1021/cm0501517.
Zhou, L., Piekiel, N., Chowdhury, S., Zachariah, M.R., 2009. T-Jump/time-of-flight mass spectrometry for time-resolved analysis of energetic materials. Rapid Commun. Mass Spectrom. 23, 194–202. https://doi.org/10.1002/rcm.3815.
Zhou, L., Piekiel, N., Chowdhury, S., Zachariah, M.R., 2010. Time-resolved mass spectrometry of the exothermic reaction between nanoaluminum and metal oxides: the role of oxygen release. J. Phys. Chem. C 114, 14269–14275. https://doi.org/10.1021/jp101146a.